



## Bioinspired Folic Acid-ADH-PLGA Polymeric Nanoparticles Loaded with Mangiferin and Piperine: A Promising Strategy for Targeted Delivery in Multidrug-Resistant Lung Cancer Cells

RITU JAIN<sup>1</sup>, RITESH TIWARI<sup>1</sup>, O.P. AGRAWAL<sup>1</sup> and AJAY KUMAR SHUKLA<sup>2,\*</sup>

<sup>1</sup>Department of Pharmaceutical Science, Madhyanchal Professional University, Bhopal-462044, India

<sup>2</sup>Department of Pharmaceutical Science, Institute of Pharmacy, Dr. Rammanohar Lohia Avadh University, Ayodhya-224001, India

\*Corresponding author: E-mail: ashukla1007@gmail.com

Received: 29 June 2023;

Accepted: 15 August 2023;

Published online: 31 October 2023;

AJC-21418

The current study aims to develop mangiferin and piperine dual drug-loaded folic acid-ADH-PLGA polymeric nanoparticles with bioinspired folic acid modifications which were effective carriers for site-specific delivery in multidrug-resistant lung cancer cells. Mangiferin and piperine, two pharmacological agents, were encapsulated within intelligent nanoparticles. These nanoparticles were fabricated utilizing folic acid, poly(lactic-co-glycolic acid) (PLGA), adipic dihydrazide (ADH) and pluronic F-68 as constituent materials. The successful fabrication of these intelligent polymeric nanoparticles was confirmed through comprehensive characterization employing various analytical techniques, including differential scanning calorimetry (DSC), Fourier transform infrared spectroscopy (FTIR), nuclear magnetic resonance (NMR) and atomic force microscopy (AFM). The efficacy of the intelligent polymeric nanoparticles against cancer cells was assessed through the evaluation of several parameters and their effectiveness was established utilizing the MTT assay. Furthermore, a hemolytic toxicity test was performed to ascertain whether the nanoparticles exerted any toxic effects on red blood cells. Mangiferin and piperine loaded FAP-M and FAP-P nanoparticles revealed a remarkable potential for inducing cell death. The findings from *in vitro* drug release assessments, hemolytic toxicity evaluations, bio-distribution analyses, MTT assays and apoptosis assessments exhibited substantial cell cycle phase arrest akin to the standard control. The comprehensive investigation and findings of the internalization process revealed the enhanced anticancer efficacy of mangiferin and piperine encapsulated in fibroblast activation protein-modified (FAP-M) and FAP-P nanoparticles as well as their biodistribution profile.

**Keywords:** Mangiferin, Piperine, Folic acid, poly(lactic-co-glycolic acid), Adipic dihydrazide, Polymeric nanoparticles.

### INTRODUCTION

Cancer, in conjunction with cardiovascular and infectious diseases, is increasingly emerging as a main global cause of mortality. Its profound impact on human health has persisted as a substantial challenge. Diligent efforts have been dedicated by numerous experts towards discovering efficacious treatments for combating this ailment. Regrettably, the mortality rate associated with cancer has shown no significant improvement over the past three decades. Consequently, there remains an exigent requirement for the development of effective and safe pharmacological interventions as well as precise methodologies for visualizing and administering anticancer therapeutics. The integration of these elements could potentially facilitate the formulation of a comprehensive strategy to combat cancer. Onco-nanotechnology, an innovative technique, represents a

novel avenue of investigation that concentrates on cancer-related phenomena and harbors significant implications. By offering a fresh perspective on the detection and analysis of cancer treatments and therapeutic strategies, onco-nanotechnology demonstrates great promise in advancing the understanding of this disease [1,2].

Chemotherapy, immunotherapy, radiation therapy and surgical excision are some of the current therapeutic modalities used to treat cancer [3]. Chemotherapy is the most cost-effective and efficient option available [4]. among them. The primary disadvantage of conventional medications, which frequently fail to differentiate between tumours and normal tissues, is poor targeted specificity. As a result, a high dose is given, which has substantial side effects (such as side effects and multidrug resistance) [5]. A powerful anticancer bioactive's parental mode of administration frequently results in severe side effects

since the medication acts on non-targeted locations. Due to this persistent drug reaction, there is less chance of the drug being absorbed at the tumour site, which causes toxicity when it enters a normal tissue as a result. The recommended dosage of a medicine cannot be successfully taken as a whole. To get over this issue, researchers are concentrating on drug combinations at specific tumour sites or drug release techniques that aim to precisely identify the delivered agents aiming towards the tumour sites [6,7].

Nano-carriers are highly efficient cancer-specific transporters owing to their inherent natural properties. The characteristic features of most tumors, including diminished lymphatic outflow and fenestrated vasculature, facilitate the retention of nanoparticles within the tumor microenvironment through the phenomenon known as enhanced permeability and retention (EPR) effect. This effect enables nanoparticles to selectively accumulate in the tumor region. Moreover, the reticuloendothelial system and mononuclear phagocytes serve as crucial physiological barriers, actively impeding the uptake of anticancer bioactive nanoparticles [8].

The nanoparticles are able to circulate for a considerable amount of time, collecting the drug everywhere around the tumour as they effortlessly escape from the fenestrated capillaries and eventually reach the tumour vasculature through improved penetration and retention effect [9]. Numerous issues plague conventional anticancer drugs, including fast clearance, a lack of selectivity and insolubility in aqueous solutions. By adopting targeted delivery of nanomaterials, which reduces the dose of drugs that must be released on the cancer cells, these difficulties can be overcome, along with non-specific toxicity towards normal cells [10]. Folic acid receptors, a potential anticancer target, are overexpressed on the surface of 40% of solid tumours but are hardly noticeable in the majority of healthy tissues [11]. By using receptor-mediated endocytosis, foliate-drug delivery systems can reach tumour cells while avoiding non-specific side effects on healthy tissues. The therapeutic chemicals were also delivered to tumour cells during this time as target cell absorption by the target cells increased [12]. They discovered that the bioactive mangiferin chemical significantly inhibited tumorigenesis and inhibited topoisomerase (MG4) hybrid cancer cell lines [13-15]. The free mangiferin solution with a lower  $IC_{50}$  was shown to be less cytotoxic to A549 cell lines than the mangiferin-loaded PLGA nanoparticles. An overview of several research was also conducted on the utilization of the mangiferin-loaded polymeric nanoparticles, with a particular focus on the enhanced bioefficacy observed in the treatment of cancer [16]. The combination of piperine with nanoparticles containing anticancer medicines has significant promise for the treatment of cancer with multidrug resistance (MDR). Due to MDR, anticancer medications may not be as effective when taken by themselves. In addition, some medications have low bioavailability because the gastrointestinal protein P-gp quickly eliminates them from the body. Piperine and nanoparticles can be used to increase the bioavailability and efficacy of anticancer medications by allowing for more effective MDR cancer treatment [15]. The anticancer activity of the compounds was enhanced by piperine emulsomes, so demonstrating the

potential of this approach for future *in vivo* investigations [17]. Mangiferin and piperine, two compounds with potential for overcoming multidrug resistance, were chosen as a representative dual drug model for post-administration applications. To achieve targeted delivery, folate receptor (FR)-targeting FA-ADH-PLGA nanoparticles loaded with mangiferin and piperine were synthesized using a polymeric conjugation method. This method significantly improved the drug-carrying capacity of nanoparticles. In order to evaluate cellular uptake, targeted drug administration and controlled release, the pharmacokinetics and pharmacodynamics of the FA-ADH-NPs were then examined. The results showed that in lung cancer, FA-ADH-NPs are a useful carrier system for enhancing the release of the mangiferin and piperine dual medication.

## EXPERIMENTAL

The dialysis membranes, folic acid (FA), pluronic F-68, poly(lactic-*co*-glycolide) (PLGA), N-hydroxysuccinimide (NHS) and dimethylaminopropylcarbodiimide hydrochloride (EDAC) were procured from Himedia Labs, Mumbai, India. Piperine, mangiferin and adipic acid dihydrazide (ADH) were procured from Sigma-Aldrich. Acetone, isopropyl alcohol and acetonitrile were acquired from Merck Ltd., India. All the chemicals used in the study were of analytical grade and used without further purification.

**Synthesis of folic acid-ADH-PLGA (FAP) copolymer:** To synthesize folic acid-based nanoparticles, a series of steps were followed using specific reagents and materials. Firstly, 50 mg of folic acid (FA) was dissolved in 5 mL of distilled water at a ratio of 10:1. To activate the functional groups of FA and facilitate interaction with other molecules, 250 mg of 1-ethyl-3-(3-dimethylaminopropyl)carbodiimide hydrochloride (EDAC) was added to the FA dispersion while stirring continuously. Subsequently, 250 mg of adipic acid dihydrazide (ADH) was introduced to the activated FA dispersion, providing a five-fold excess of the ligand. The mixture was allowed to react at room temperature for up to 8 h. In addition, poly(lactic-*co*-glycolic acid) (PLGA) were weighing 50 mg was dispersed in 10 mL of acetone. To initiate the formation of PLGA dispersion, 100 mg of dicyclohexylcarbodiimide (DCC) and 50 mg of N-hydroxysuccinimide (NHS) were added to the solution under continuous stirring for 10 h. Once the PLGA dispersion was formed, it was then carefully dropped into the FA-ADH-NH<sub>2</sub> solution and stirred for an additional 8 h. This step ensured the proper and uniform interaction between the amine groups of ADH-NH<sub>2</sub> and the carboxyl groups (-COOH) of PLGA, leading to the formation of carbodiimide conjugation. Consequently, FA-ADH-NH<sub>2</sub> bound to the polymer PLGA-COOH. The resulting copolymer, named folic acid-ADH-PLGA (FAP), was then subjected to vacuum drying and subsequently analyzed using <sup>1</sup>H NMR spectroscopy (Bruker DRX, 400 MHz) and FTIR spectroscopy (IR Tracer-100, Shimadzu).

**Synthesis of FA-ADH-PLGA nanoparticles using FA-ADH-PLGA copolymer (FAP) and plain polymeric nanoparticles (PLGA nanoparticle):** The FA-ADH-PLGA (FAP) copolymer (10-30 mg) was dissolved in 20 mL of acetone. Drug (mangiferin and piperine) (30 mg) was dissolved in acetone

and added to the FA-ADH-PLGA (FAP) solution that was made. Meanwhile, pluronic (F-68) was dissolved in distilled water to make different concentrations of 0.5%, 1% and 2%. Folic acid-ADH-PLGA (FAP) copolymer solution was added to pluronic F-68 solution dropwise over the course of 5 h while being constantly stirred. After that, the nanoparticle dispersion was separated using a membrane filter (0.45  $\mu\text{m}$ ) and centrifuged (C-24, BL, Remi, Mumbai, India) for 15 min at 10,000 rpm. After centrifugation, the FA-ADH-PLGA nanoparticles (FAP NPs) were lyophilized for further use after the supernatant was taken out. The piperine- and mangiferin-encapsulated FAP nanoparticles are referred to as FAP-M and FAP-P, respectively.

It was possible to dissolve 50 mL into ordinary polymeric (PLGA) nanoparticles by employing the previously mentioned method. Then dicyclohexylcarbodiimide (100 mg) and N-hydroxysuccinimide (50 mg) were added with constant stirring for 10 h after PLGA (50 mg) was dispersed in acetone (10 mL). After pluronic (F-68) was dissolved in distilled water and three different pluronic concentrations (0.5%, 1% and 2%) were formed, mangiferin (30 mg) was added to the PLGA solution. PLGA solution was added to pluronic F-68 solution dropwise for 5 h while being constantly stirred. A membrane filter (0.45  $\mu\text{m}$ ) was used to separate the PLGA nanoparticle dispersion and the mixture was subsequently centrifuged for 15 min at 10,000 rpm. After centrifugation, the PLGA nanoparticles were lyophilized for later use and the supernatant was discarded. For upcoming study, PLGA NPs and FAP NPs were lyophilized and preserved.

### Characterization parameters of FAP nanoparticles and PLGA nanoparticles

**Surface morphology:** Atomic force microscopy (AFM) Alpha-300RA was used to examine the surface morphology of the synthesized compounds. The SEM-1400 TEM (Jeol, Japan analytical electronic microscope) was used to evaluate the morphological parameters at 80 kV in order to identify the surface morphology using TEM.

**Zeta potential and particle size analysis:** The particle size and zeta potential of the synthesized nanoparticles were determined using the Malvern device (DTS Ver. 4.10, Malvern Instruments, WR14 1XZ, UK).

**DSC analysis:** The significance of nanoparticles was assessed by differential scanning calorimetry utilizing a DSC 60 device (Shimadzu, Kyoto, Japan). The 10mg samples of the drugs (FA, Mangiferin, Piperine, Plain FAP, Mangiferin-loaded FAP NPs and Piperine-loaded FAP NPs) were placed in the aluminium pan and the DSC thermogram was observed at a scanning temperature range of up to 300 °C with a heating rate of 10 °C/min in a nitrogen atmosphere.

**Entrapment proficiency analysis:** A Shimadzu LC-10AT HPLC, SPD-20A UV detector and Inertsil ODS-SP column (250 4.6 mm, 5 m) was used for the chromatographic analysis. An aqueous solution of methanol containing 0.1% phosphoric acid constituted as mobile phase (31:69, v/v). For the detection of mangiferin-loaded system (FAP-M NPs), the analyses were carried out at a flow rate of 1.0 mL/min with ultraviolet (UV) detection at 258 nm, while for the detection of piperine-loaded

system (FAP-P NPs), the flow rate was 1 mL/min with a wavelength of 353 nm. The procedure was carried out at ambient temperature. About 10 mg FAP NPs and PLGA NPs loaded with piperine and mangiferin were dispersed in acetone. After centrifuging the dispersion for 12 min at 10,000 rpm, the foreign polymeric substances was separated from the supernatant. The clear supernatant solution was examined by HPLC at 415 nm and 342 nm, respectively, to ascertain the amount of loaded mangiferin and piperine in the developed FAP nanoparticle system [18-20].

**In vitro drug release studies:** A 50 mL of phosphate buffer saline (PBS) solution having pH 7.4 was added 50 mL of FAP-M and FAP-P NPs separately, as well as plain mangiferin and plain piperine, dialysis bags (Himedia) and these solutions were continuously stirred at 100 rpm in oven at 37 °C. At certain intervals, 1 mL of buffer solution was taken out and replaced with the same volume of new buffer solution. The amount of drug released from nanoparticles was measured using an HPLC system (Wasters HPLC, Model 515) [21].

**Hemolytic toxicity studies:** The human blood was obtained from an accredited pathology laboratory using anti-coagulant vials. The collected blood sample was centrifuged and the resulting red blood cells (RBCs) were extracted and diluted by mixing 1 mL of RBCs with 5 mL of distilled water. This diluted solution served as a 100% hemolytic standard.

To conduct the spectrophotometric measurements, the generated 100% hemolytic solutions were employed as blanks and divided into four tubes, each containing a standard hematocrit solution. The first tube received a plain drug solution of mangiferin, the second tube received a plain drug solution of piperine, the third tube was supplemented with FAP-M NPs and the fourth tube contained piperine loaded FAP NPs. These tubes were then treated with erythrocyte suspension. Subsequently, the solution was centrifuged for 10 min at 5000 rpm and the absorbance of the resulting supernatants was measured at 540 nm. This absorbance value was utilized as a 100% hemolytic standard for quantifying the percentage of hemolysis [18].

**Bio-distribution analysis:** In this investigation, albino rats weighing 120  $\pm$  20 g were employed to investigate the bio-distribution of an anticancer medication comprising piperine and mangiferin. The animals were divided into four groups, each consisting of six animals. The first group received an infusion of plain mangiferin solution, while the second group received an infusion of plain piperine solution. The third group was administered mangiferin loaded FAP NPs *via* the intraperitoneal route and the fourth group received piperine loaded FAP NPs. All animals in each group were sacrificed after 2 hours, and their internal organs were removed, which include liver, lungs, spleen, heart, stomach, kidneys and intestines. These organs were subsequently homogenized in phosphate-buffered saline (PBS) at pH 7.4. To remove proteins, acetonitrile was utilized for deproteinization of the homogenates. The resulting homogenates were then subjected to filtration and centrifugation, then the drug content was determined using HPLC method [22,23].

**Blood level study:** Plasma drug levels in albino rats were assessed subsequent to intravenous administration of plain

piperine, mangiferin and FAP NPs solution (mangiferin and piperine loaded). Four distinct groups of albino rats were generated for each synthesized nanoparticle, comprising six rats per group. The initial and second groups were subjected to intravenous administration of a plain solution of mangiferin (20 mg/kg body weight) and FAP NPs (loaded with mangiferin), respectively. The third and fourth groups received intravenous administration of a plain solution of piperine (20 mg/kg body weight) and FAP NPs (loaded with piperine), respectively. After the sample administration, 0.1 mL of blood was collected from the retro-orbital plexus of each albino rat in each group at the intervals of 1, 2, 4, 6 and 8 h, up to a duration of 24 h. The blood samples were then subjected to centrifugation at 5000 rpm for 10 min, following which the resulting supernatant (serum) was obtained and deproteinized using a specified quantity of acetonitrile (1 mL/mL of serum). Finally, the drug concentration in the supernatants was determined using HPLC analysis of the acquired samples [22].

**MTT assay for cell cytotoxicity evaluation:** The A549 cell line, derived from human alveolar lung cancer, was obtained from NCCS, Pune, India. These cells were cultivated in DMEM high glucose medium supplemented with 10% fetal bovine serum (FBS) and 1% antibiotic-antimycotic solution. The incubation was performed in a CO<sub>2</sub> incubator with an atmosphere containing 18-20% oxygen at 37 °C. The sub-culturing of the cells was performed every 2 days.

A 200 µL solution containing the desired cell density (20,000 cells/well) was seeded into a 96-well plate, excluding the presence of the test agent. The cells were allowed to grow for approximately 24 h and then the test sample was added at the specified concentrations. The plate was incubated for 24 h at 37 °C in 5% CO<sub>2</sub> atmosphere. After the completion of incubation period, the plates were removed from the incubator and the supernatant was discarded. MTT reagent was added to achieve a final concentration of 0.5 mg/mL in the total volume. To prevent light-induced reactions, the plate was covered with aluminum foil and again incubated for an additional 3 h. Following this, the MTT reagent was removed and 100 µL of DMSO was added. The absorbance at 570 nm was measured using a spectrophotometer or an ELISA reader. The IC<sub>50</sub> value, which represents the concentration at which the test agent inhibits 50% of cell viability, was calculated using a linear regression equation of the form  $y = mx + C$ . The formula for determining percent cell viability was employed accordingly:

$$\text{Cell viability (\%)} = \frac{\text{Absorbance of treated cells}}{\text{Absorbance of untreated cells}} \times 100$$

**Apoptosis assay:** The cell lines used in this study were acquired from NCCS, Pune, India and the cells were cultured in DMEM supplemented with 10% inactivated fetal bovine serum (FBS), penicillin (100 IU/mL) and streptomycin (100 g/mL). The cells were maintained at 37 °C in the presence of 5% CO<sub>2</sub> environment. A cell dissociating solution containing 0.2% trypsin, 0.02% EDTA and 0.05% glucose in PBS was employed to separate the cells. Cell viability was assessed and the cells were subsequently centrifuged. Additionally, 50,000 cells per well were seeded in a six-well plate and incubated

for 24 h at 37 °C containing 5% CO<sub>2</sub>. To prepare the monolayer cell culture, the cells were trypsinized from the monolayer and adjusted to  $0.5 \times 10^6$  cells/mL using an appropriate medium containing 10% FBS in DMEM medium. A volume of 2000 µL of diluted cell suspension ( $0.5 \times 10^6$  cells/well) was added to each well of the six-well microtiter plate. After 24 h, when a partial monolayer had formed, the supernatant was removed and the monolayer was washed once with medium. Then, the test compounds at the appropriate concentration (IC<sub>50</sub>) were applied to the partial monolayer on the microtiter plates along with the standard control. Negative controls comprised the untreated cells. Following the incubation period, the test solutions were removed from the wells and the cells were rinsed with phosphate-buffered saline (PBS). The PBS was then aspirated and a 200 µL of trypsin-EDTA solution was added. The cells were allowed to incubate at 37 °C for a duration of 3-4 min. The culture medium was returned to the respective wells and the cells were promptly collected into 5 mL polystyrene tubes. Subsequently, the tubes were subjected to centrifugation at 1800 rpm for 5 min. The cells were then washed with PBS and subjected to another round of centrifugation at 1800 rpm for 5 min. To fix and permeabilize the cells, the pre-chilled 70% pure ethanol stored at -20 °C for 30-40 min. The cells were stained with 400 µL of propidium iodide/RNase staining buffer and incubated at room temperature in the absence of light for 30 min. The cells were then incubated in the dark at room temperature for 30 min with 5 µL of Annexin-V FITC and 5 µL of propidium iodide. Flow cytometry was employed to analyze the samples, which were diluted in 400 µL of annexin V binding buffer. The data obtained from this process were analyzed using BD FACS Calibur equipped with BD Cell Quest Pro Software [24-26].

**Statistical analysis:** The study findings were presented as mean SD. The t-test was used to make this assessment and  $p < 0.05$  was also significant. All the experiments were carried out three times.

## RESULTS AND DISCUSSION

This research sought to evaluate the anticancer effects of a mangiferin and piperine-loaded, folate-appended PLGA nanoparticulate system on human lung cancer cells (A549).

**FTIR studies:** The FAP copolymer underwent validation through the utilization of <sup>1</sup>H NMR and FTIR spectroscopic analyses. Fig. 1 illustrates a graphical representation of the obtained <sup>1</sup>H NMR and FTIR spectra. The characteristic peaks were identified in the FTIR spectra, including a peak at 3250 cm<sup>-1</sup>, attributed to the stretching of N-H bonds in the amide group. The peaks at 2150 and 1250 cm<sup>-1</sup> revealed the presence of C-H bonds in the alkene bridge. A peak at 1640 cm<sup>-1</sup> appeared as a result of the stretching of C=O bonds. Additionally, a peak at 1480 cm<sup>-1</sup> indicated the stretching of C-N bonds in the amide linkage, while a peak at 991 cm<sup>-1</sup> signified the presence of C=O stretching. The appearance of distinct peaks at 3250 and 1640 cm<sup>-1</sup> supported the formation of an amide junction and an amide bond, respectively, as well as the existence of a C=O carboxyl linkage bonded to the amine group of ADH with the -COOH and -OH groups of FA and PLGA, respectively.

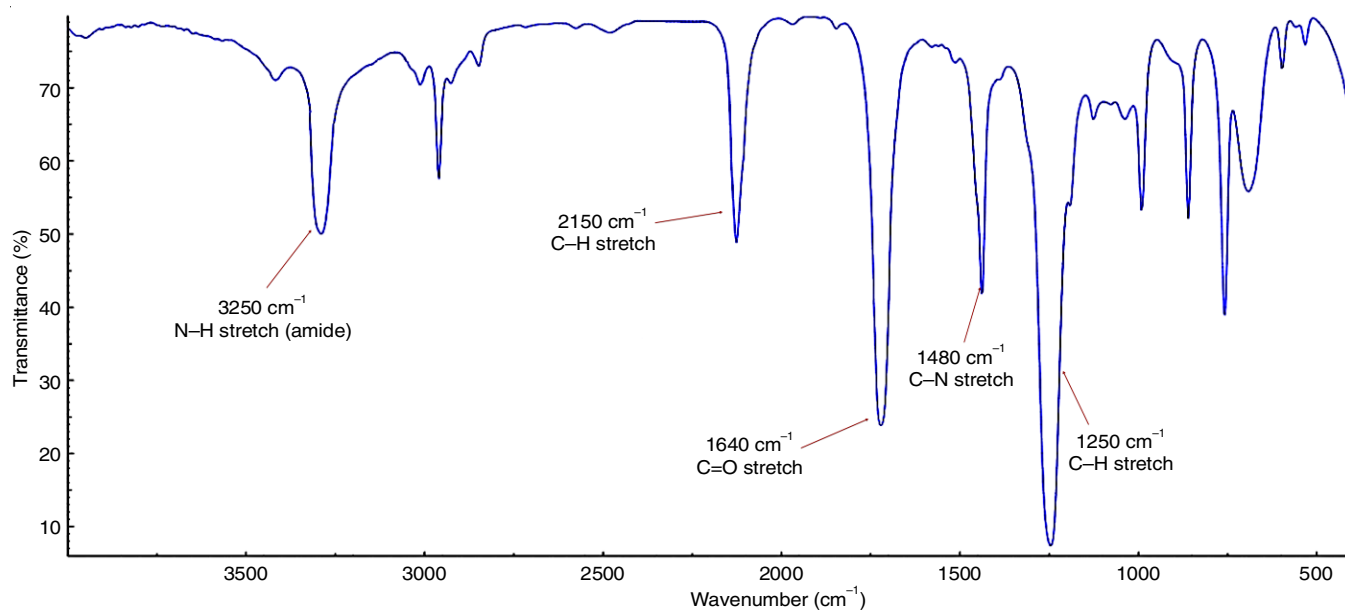


Fig. 1. FTIR spectrum of FAP copolymer

These observations provided evidence for the presence of an amide bond and a C=O carboxyl linkage.

**<sup>1</sup>H NMR studies:** The presence of folic acid (FA), adipic acid dihydrazide (ADH) and poly(lactic-co-glycolic acid) (PLGA) in the FAP copolymer is evidenced by the presence of comparable peaks in the <sup>1</sup>H NMR spectrum. The following NMR results were obtained for the produced FAP copolymer: chemical shift values ( $\delta$ ) ranging from 1.43 to 1.63 ppm representing 7 hydrogen atoms, with specific values of 1.49 ppm (doublet,  $J = 7.4$  Hz), 1.55 ppm (quintet,  $J = 7.4$  Hz), 1.55 ppm (quintet,  $J = 7.4$  Hz), 1.57 ppm (quintet,  $J = 7.4$  Hz) and 1.57 ppm (quintet,  $J = 7.4$  Hz); whereas the chemical shift values ranging from 1.85 to 1.97 ppm representing 2 hydrogen atoms, with specific values of 1.91 ppm (quartet,  $J = 7.3$  Hz) and 1.91 ppm (quartet,  $J = 7.3$  Hz). The chemical shift of 2.33-2.49 ppm is attributed to FA, while the chemical shift of 4.34-6.96 ppm corresponds to PLGA and FAP.

**Surface characteristics:** The nanostructures possessed a circular shape and fall within the nanoscale size range as depicted in Fig. 2a-b. The AFM technique was used to observe the nanoparticles and it was discovered that their sizes exhibited an extensive degree of uniformity, which provided insights on the dimensions of the nanoparticles. In the photomicrograph resulting from AFM analysis, the nanostructures are uniformly

grouped and exhibit consistent peaks. A high-resolution transmission electron microscopy (TEM) image illustrates the nanoscale diameter range of the formulation as shown in Fig. 2c-d. A homogenous distribution and distinct pattern in the polymeric nanoparticle formulation will enhance dispersibility.

**Surface potential, particle size and % drug entrapment:**

A particle size analyzer was used to measure the dimensions of the nanoparticles of FAP nanoparticles and the particle size of FAP-M nanoparticles was found to be 93 nm. As shown in Table-1, the particle size increased from 93 nm to 189 nm as the copolymer and medicine mangiferin concentrations were increased. The size of the FAP-P nanoparticles was found to be 98 nm. The particle size increased from 99 nm to 205 nm when the quantity of copolymer and drug piperine was increased (Table-2).

As demonstrated in Tables 1 and 2, different surfactant concentrations and medication dosages were used to modify nanoparticle size. The size of FAP-M and FAP-P particles increases when the amount of pluronic is increased from 1% to 2%, but the effectiveness of entrapment (drug content) decreases. The entrapment was decreased from 94.33% to 76.78% as the particle size of FAP-M NPs increased from 93 nm to 189nm. Similar to this, entrapment decreased (from 91.87% to 74.55%) as particle size (FAP-P) increased from 98 nm to 205 nm. This

TABLE-1  
CONSTITUENTS AND QUANTITY USED IN THE SYNTHESIS OF FAP-M NANOPARTICLES

S. No.	FAP:Drug ratio (mg)	Dispersed phase			Dispersion medium		Entrapment efficiency (%)	Particle size (nm)
		FAP (mg)	Mangiferin (mg)	Acetone:IPA (9:1) (mL)	Pluronic F-68 (mg)	Water (mL)		
M1	20:10	20	10	20	200	20	78.40 $\pm$ 0.75	181 $\pm$ 1.98
M2	20:20	20	20	20	200	20	86.52 $\pm$ 1.15	141 $\pm$ 1.25
M3	20:30	20	30	20	200	20	94.33 $\pm$ 1.98	93 $\pm$ 0.75
M4	20:10	20	10	20	400	20	76.78 $\pm$ 0.50	189 $\pm$ 2.25
M5	20:20	20	20	20	400	20	84.35 $\pm$ 0.95	163 $\pm$ 1.50
M6	20:30	20	30	20	400	20	90.54 $\pm$ 1.55	115 $\pm$ 1.15

M1-M6: Formulation (represents mangiferin); FAP: Folic acid-ADH-PLGA copolymer; FA: Folic acid.

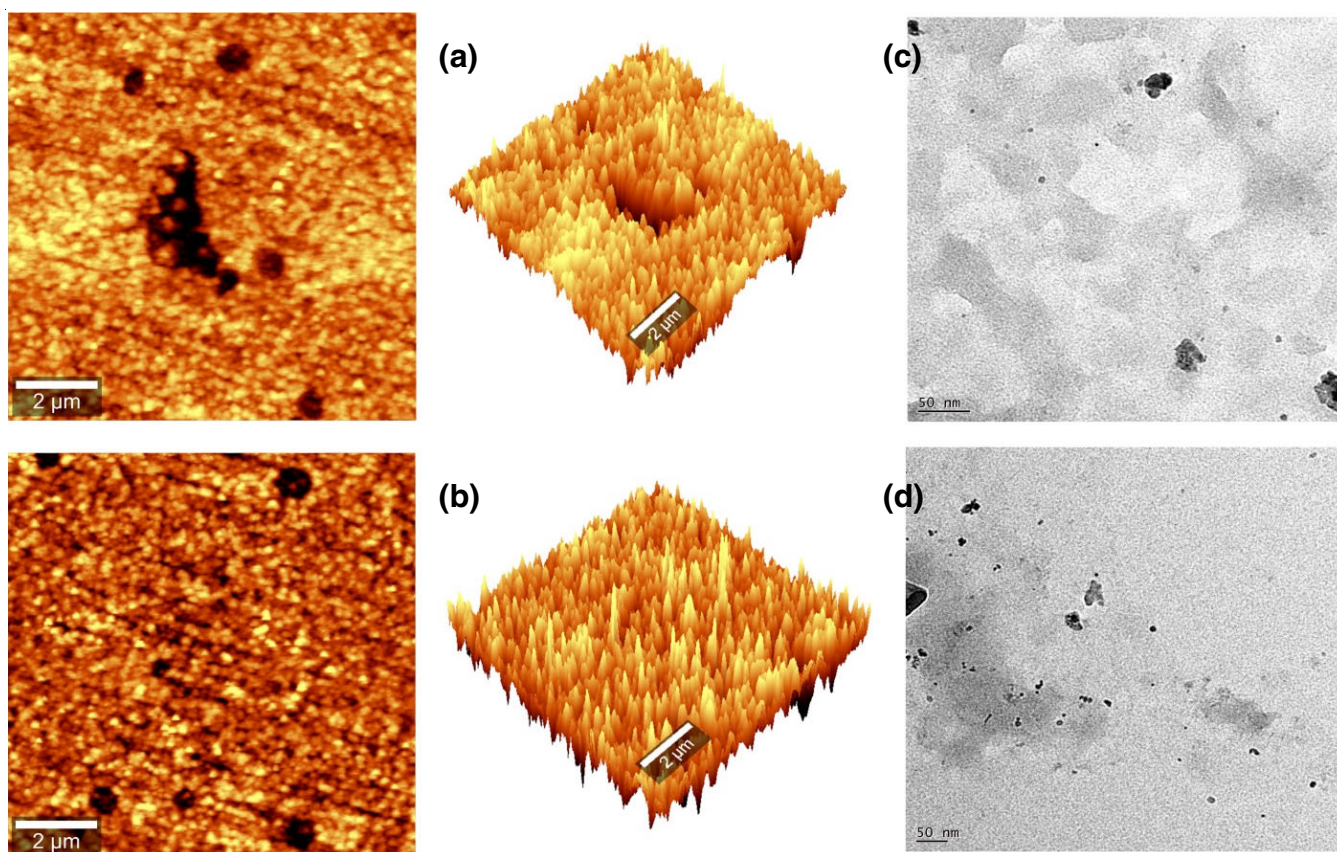


Fig. 2. 2D and 3D-AFM image of FAP nanoparticles. (a) FAP-M; (b) FAP-P; TEM image of FAP nanoparticles. (c) FAP-M; (d) FAP-P

TABLE-2  
CONSTITUENTS AND QUANTITY USED IN THE SYNTHESIS OF FAP-P NANOPARTICLES

S. No.	FAP:Drug ratio (mg)	Dispersed phase			Dispersion medium		Entrapment efficiency (%)	Particle size (nm)
		FAP (mg)	Piperine (mg)	Acetone:IPA (9:1) (mL)	Pluronic F-68 (mg)	Water (mL)		
P1	20:10	20	10	20	200	20	76.38 ± 0.70	193 ± 1.80
P2	20:20	20	20	20	200	20	83.46 ± 1.10	165 ± 1.50
P3	20:30	20	30	20	200	20	91.87 ± 1.50	98 ± 1.12
P4	20:10	20	10	20	400	20	74.55 ± 0.45	205 ± 2.00
P5	20:20	20	20	20	400	20	80.89 ± 0.75	178 ± 1.65
P6	20:30	20	30	20	400	20	86.98 ± 1.25	143 ± 1.25

P1-P6: Formulation (represents piperine); FAP: Folic acid-ADH-PLGA copolymer; FA: Folic acid.

suggests that encapsulation efficiency decreases as particle size increases. As a result, both particle size and the percentage of drug loading are significantly influenced by the surfactant content (pluronic F-68) and raising the surfactant concentration from 1% to 2% may change both the size of the particles and the entrapment effectiveness of FAP nanoparticles.

The FAP-M nanoparticles exhibited a polydispersity index (PDI) of  $0.074 \pm 0.04$ , while the FAP-P nanoparticles demonstrated a PDI index of  $0.075 \pm 0.06$ . It is known that polydisperse nanoparticles typically exhibit PDI values ranging from 0.5

to 0.7, indicating a broad distribution of particle sizes. In this study, both FAP-M and FAP-P nanoparticles displayed PDI values below 0.7, suggesting a narrower range of particle sizes. Danaei *et al.* [27] determined the entrapment effectiveness of the synthesized FAP-M and FAP-P nanoparticles, which was found to be 94.33% and 91.87%, respectively. Additionally, the zeta potential of FAP-M nanoparticles was found to be -12.8 mV, while FAP-P nanoparticles displayed a zeta potential of -11.5 mV (Table-3). This negative zeta potential can be attributed to the presence of the -OH group in the PLGA

TABLE-3  
OPTIMIZED PARTICLE SIZE & ENTRAPMENT EFFICIENCY OF FAP-M AND FAP-P NANOPARTICLES

Formulations	Entrapment efficiency	Particle size (nm)	Polydispersity index	Zeta potential
FAP-M NPs	94.33 ± 1.98	93 ± 0.75	0.074 ± 0.04	-12.8 mV
FAP-P NPs	91.87 ± 1.50	98 ± 1.12	0.075 ± 0.06	-11.5 mV

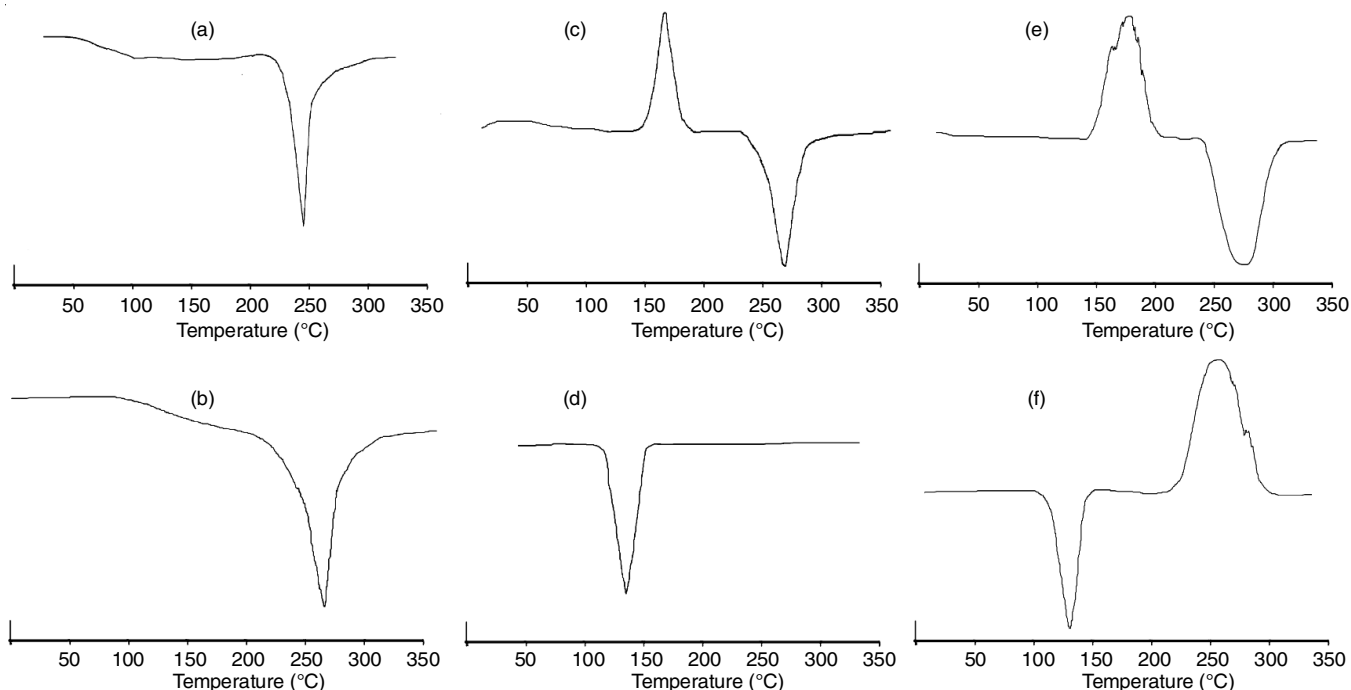


Fig. 3. DSC thermogram: (a) folic acid (FA); (b) PLGA; (c) mangiferin; (d) piperine; (e) FAP-M and (f) FAP-P

and the  $-\text{COOH}$  group in the ligand folic acid (FA) attached to the nanoparticles. Charged nanoparticles with higher zeta potentials tend to form more stable and persistent particles due to increased repulsive interactions. Therefore, the slightly lower negative electrostatic charge observed in the FAP-M and FAP-P nanoparticles contributes to the improved stability of the nanoparticle system.

**DSC studies:** Differential scanning calorimetry (DSC) thermograms were generated and depicted in Fig. 3 to analyze the thermal behaviour of various compounds including folic acid (FA), poly(lactic-co-glycolic acid) (PLGA), mangiferin, piperine, mangiferin-loaded FAP nanoparticles (FAP-M NPs) and piperine-loaded FAP nanoparticles (FAP-P NPs). Ferulic acid exhibited an endothermic peak at 242 °C, indicating a unique thermal transition specific to ferulic acid. PLGA demonstrated an endergonic peak at 270 °C. Mangiferin displayed an endothermic peak at 253 °C along with an exergonic peak at 180 °C. In the case of FAP-M NPs, the thermogram revealed a thermally activated peak corresponding to folic acid at 245 °C. Moreover, an endothermic peak and an exothermic peak corresponding to mangiferin were observed at 255 and 180 °C, respectively. Additionally, the thermograms exhibited an exothermic peak at 275 °C indicating the presence of PLGA in the nanostructures of FAP-M NPs, thereby confirmed the incorporation of mangiferin in FAP NPs. Furthermore, the DSC thermogram of FAP-P NPs exhibited an exothermic peak at 140 °C suggesting that piperine exists in a crystal-like form within the nanoparticle matrix. These findings from the DSC thermograms of FAP-P NPs provide evidence of the presence of piperine in the nanoparticle formulation.

**In vitro drug release pattern:** The drug release profile depicted in Fig. 4 illustrates the sustained and prolonged release of mangiferin and piperine from a nanoparticle system com-

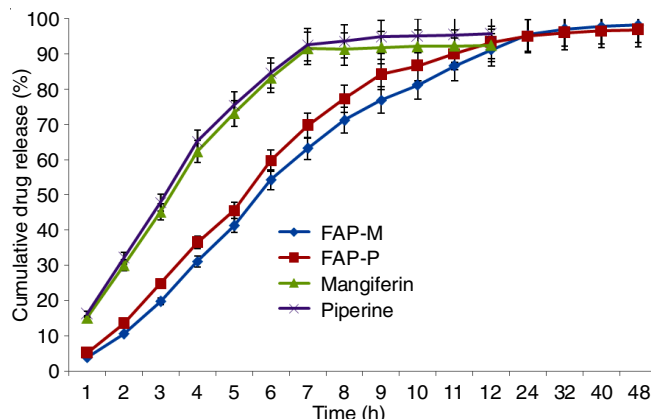


Fig. 4. Percentage cumulative drug release of FAP-M and FAP-P NPs

prising FAP-M and FAP-P, respectively. The drug release graph showed a comparison between the release patterns of unmodified mangiferin and piperine and the controlled, long-term release of these compounds from the FAP-M and FAP-P nanoparticulate systems. In case of mangiferin and piperine, 92.45% and 95.69% of the compounds were released within a 24 h, respectively. Conversely, mangiferin and piperine encapsulated within the FAP-M and FAP-P nanoparticles exhibited a release profile extended to 48 h, with release percentages of 98.2% and 96.9%, respectively. This enhanced release behaviour can be attributed to the choice of suitable solvents, namely acetone and isopropanol, employed during the manufacturing process of the nanoparticle carriers. These solvents likely facilitate the disruption of folic acid hydrogen bond and promote the interaction between the carboxyl group ( $-\text{COOH}$ ) of folic acid and the amine group ( $-\text{NH}_2$ ) of adipic acid dihydrazide (carbodi-imide conjugation). This interaction leads to the formation of covalently bonded core-shell micelles with reduced solubility.

TABLE-4  
DATA OF ABSORBANCE OF 10% HEMATOCRIT SOLUTION AT 540 nm

10% Hematocrit solution	Absorbance at 540 nm	Cumulative drug release (%)
10% Hematocrit solution of distilled water with mangiferin	0.1648	12.15
10% Hematocrit solution of distilled water with piperine	0.1610	14.17
10% Hematocrit solution of distilled water with FAP-M NPs	0.1823	2.82
10% Hematocrit solution of distilled water with FAP-P NPs	0.1778	5.22

**Hemolytic toxicity study:** To investigate the hemotoxic effects of the constructed FAP (flavonoid-ascorbic acid-phospholipid) nanoparticle, a hemolytic toxicity study was conducted. The hemolytic toxicity of plain mangiferin, piperine, FAP-M NPs and FAP-P NPs was assessed and found to be 12.15%, 14.17%, 2.82% and 5.22%, respectively, when dissolved in distilled water. The extended release of the bioactive compounds from the nanoparticles resulted in a decrease in hemolytic toxicity. According to the results of the hemolytic toxicity study, FAP-M and FAP-P NPs exhibited lower toxicity compared to plain mangiferin and piperine, respectively (Table-4). This may be attributed to the hydrophilic properties of flavonoid-ascorbic acid, which create a hemocompatible environment. The reduction of medication-induced hemotoxicity observed in this study may have implications based on previous similar studies involving nanoparticle formulations [28].

**In vivo bio-distribution study:** A biodistribution study was conducted to assess the distribution of medication within different organs including the liver, lung, spleen, heart, stomach, intestine and kidney. After 2 h, the administration of a mangiferin drug solution, the amount of drug released and identified in the liver, spleen, heart, stomach, intestine, kidney and lungs was found to be 9.66%, 5.56%, 7.12%, 2.55%, 8.69%, 6.98% and 2.71% respectively. Similarly, after 2 h, the levels of piperine were determined to be 10.22%, 6.25%, 7.55%, 2.85%, 8.99%, 7.46% and 2.8% in the liver, spleen, heart, stomach, intestine, kidney and lungs, respectively. In case of FAP-M, a higher percentage of mangiferin was observed in lung (8.12%), liver (2.52%), spleen (1.88%), heart (4.15%), stomach (1.91%), intestine (2.14%) and kidney (2.98%). Similarly, for FAP-P, a greater percentage of piperine was found in lung (7.65%), liver (2.54%), spleen (1.95%), heart (4.33%), stomach (2.15%), intestine (2.35%) and kidney (3.16%). The levels of mangiferin and piperine in the body are influenced by their release, dispersion and breakdown within the system. Notably, in case of the unencapsulated drug, a higher amount of free drug was observed in the liver. However, the FAP-M and FAP-P nanoparticles significantly reduced the fraction of drug accumulated in the liver. This can be attributed to the hydrophilic nature of folate, which allows FAP nanoparticles to circulate for longer periods, persist in the bloodstream and hinder entry into the liver. Consequently, the potential liver toxicity associated with the conventional medication can be minimized. Fig. 5 illustrates the biodistribution pattern of mangiferin and piperine from FAP-M and FAP-P nanoparticles.

**Blood level study:** The present study aimed to investigate the blood level dynamics of mangiferin and piperine-loaded FAP NPs formulations following intravenous (IV) administration in an animal model (albino rats) in order to evaluate the

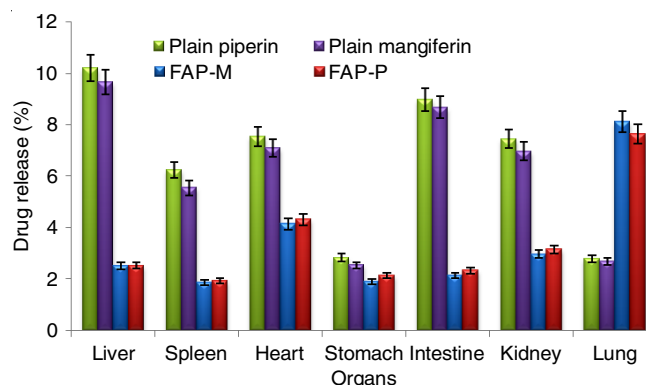


Fig. 5. Biodistribution pattern of mangiferin, piperine in different organs after administration of FAP-M and FAP-P NPs formulations

efficacy of transporting these compounds into the bloodstream. Fig. 6 illustrates the temporal changes in serum concentrations of mangiferin and piperine-loaded FAP NPs formulations. It was observed that FAP-M and FAP-P NPs significantly enhanced the blood concentrations of mangiferin and piperine compared to their respective plain solutions.

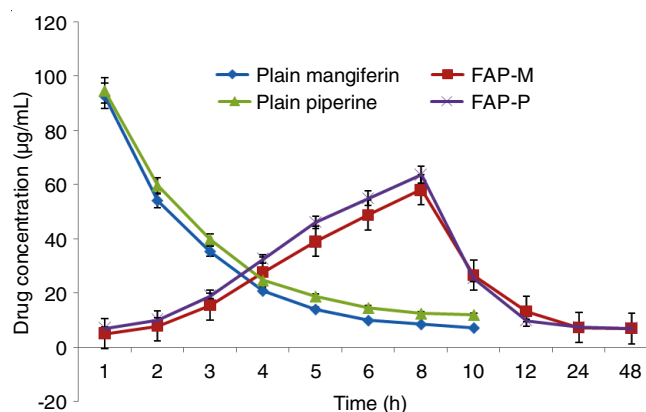


Fig. 6. Concentration of mangiferin and piperine in serum after IV administration of FAP-M and FAP-P NPs formulations in albino rats

In the serum analysis, the highest proportion of mangiferin solution in the blood was recorded at 92.65% after 1 h, which subsequently declined to 7.15% over the course of experiment. The initial concentration of mangiferin in the blood following administration of FAP-M NPs was 4.98%, which increased to 58.12% after 8 h and gradually decreased to 6.85% after 48 h. Similarly, in serum analysis, the highest proportion of mangiferin and piperine was observed at 94.54% after 1 h, followed by a gradual decrease to 11.58% over time. The initial concentration of mangiferin and piperine in the blood following administration of FAP-P NPs was 6.87%, which increased to 63.54% after 8 h and gradually decreased to 7.12% after 48 h. The

sustained release of mangiferin and piperine was facilitated by folate-anchored PLGA NPs, owing to the hydrophilic folate coating on PLGA, which promotes pro-longed circulation in the bloodstream.

**MTT assay:** The A549 cell line was utilized to conduct an *in vitro* cytotoxicity assessment of nanomaterials using the MTT assay. The experimental results indicate a dose-dependent evaluation of cytotoxic effects, wherein the systemic bio-availability decreases as the concentration of the samples (FAP-M and FAP-P NPs) increases. Statistical analysis of the MTT cytotoxicity study reveals significant cytotoxic potential of the test compounds, namely F1 (FAP-M) and F2 (FAP-P), against the A549 cell lines, with  $IC_{50}$  concentrations of 17.68  $\mu\text{g/mL}$  and 34.53  $\mu\text{g/mL}$ , respectively (Table-5). Both F1 and F2 compounds exhibit effective cytotoxicity against A549 cells, suggesting their potential as potent agents for lung cancer treatment due to their low  $IC_{50}$  values on A549 cells. The graph (Figs. 7 and 8) illustrates the impact of the percentage inhibition of the cell growth.

Sample code	$IC_{50}$ ( $\mu\text{g/mL}$ )
F1	17.68
F2	34.53

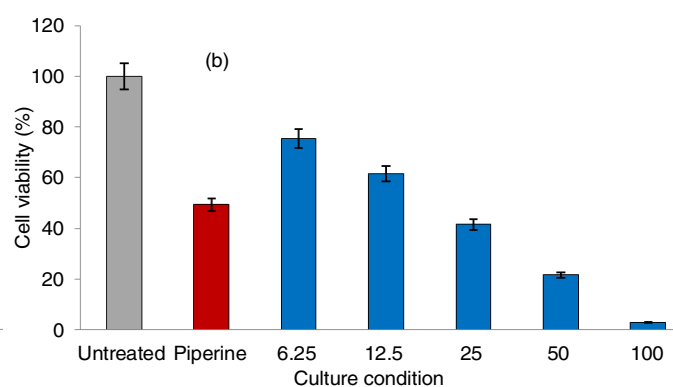
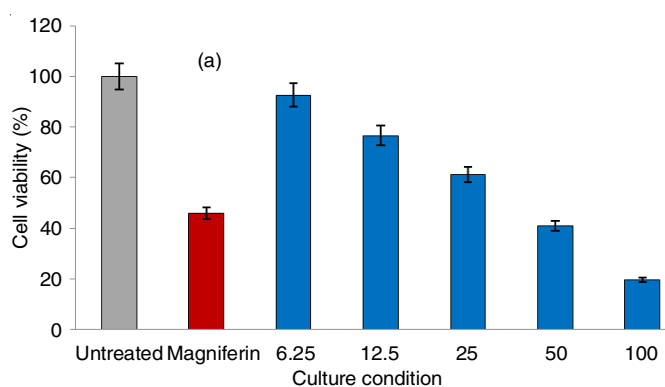


Fig. 7. *In vitro* percentage control growth of A549 cancer cellline against (a) FAP-M NPs; (b) FAP-P NPs

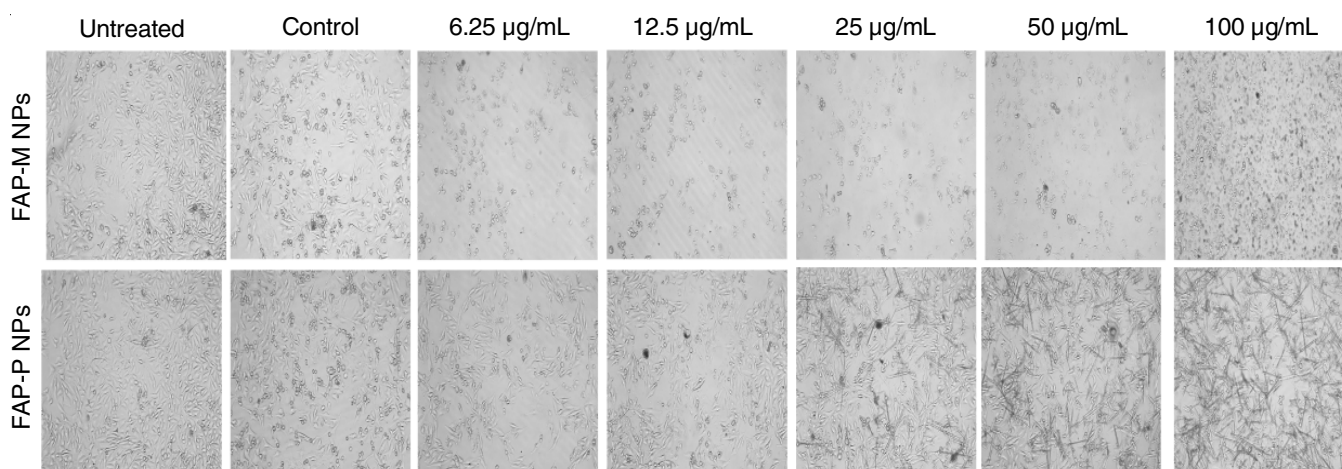


Fig. 8. Photomicrograph of *in vitro* percentage control growth of A549 cancer cellline against (a) FAP-M NPs; (b) FAP-P NPs

The findings show that greater nanoparticles concentrations prevent the cell development. Moreover, the cell survival increases along with the amount of nanoparticles. Thus, FAP-M and FAP-P NPs compositions were found to be more cytotoxic when compared to the conventional mangiferin and piperine at dosages ranging from 6.25 to 100  $\mu\text{g/mL}$ .

**Cell cycle investigation:** In comparison to untreated cells, cells treated with standard, control and test material FAP-M and FAP-P NPs) at  $IC_{50}$  values (Table-6) show a large percentage of DNA at G2/M and S stage arrest. In contrast to FAP-P NPs, which efficiently arrests cells in the Sub G0/G1, S and G2/M phases (Fig. 9), FAP-M effectively arrests cell populations in the G2/M phase. As a result, at the G2/M and S phases, the cell cycle effectively came to an end. After receiving mangiferin, A549 cells showed considerable cell cycle phase arrest, comparable to the typical control.

Cell cycle stage	Untreated	Control	FAP-M	FAP-P
Sub G0/G1	0.56	1.91	1.67	10.07
G0/G1	88.72	28.95	30.75	41.47
S	1.3	12.26	15.41	25.53
G2/M	8.99	40.64	33.02	17.75

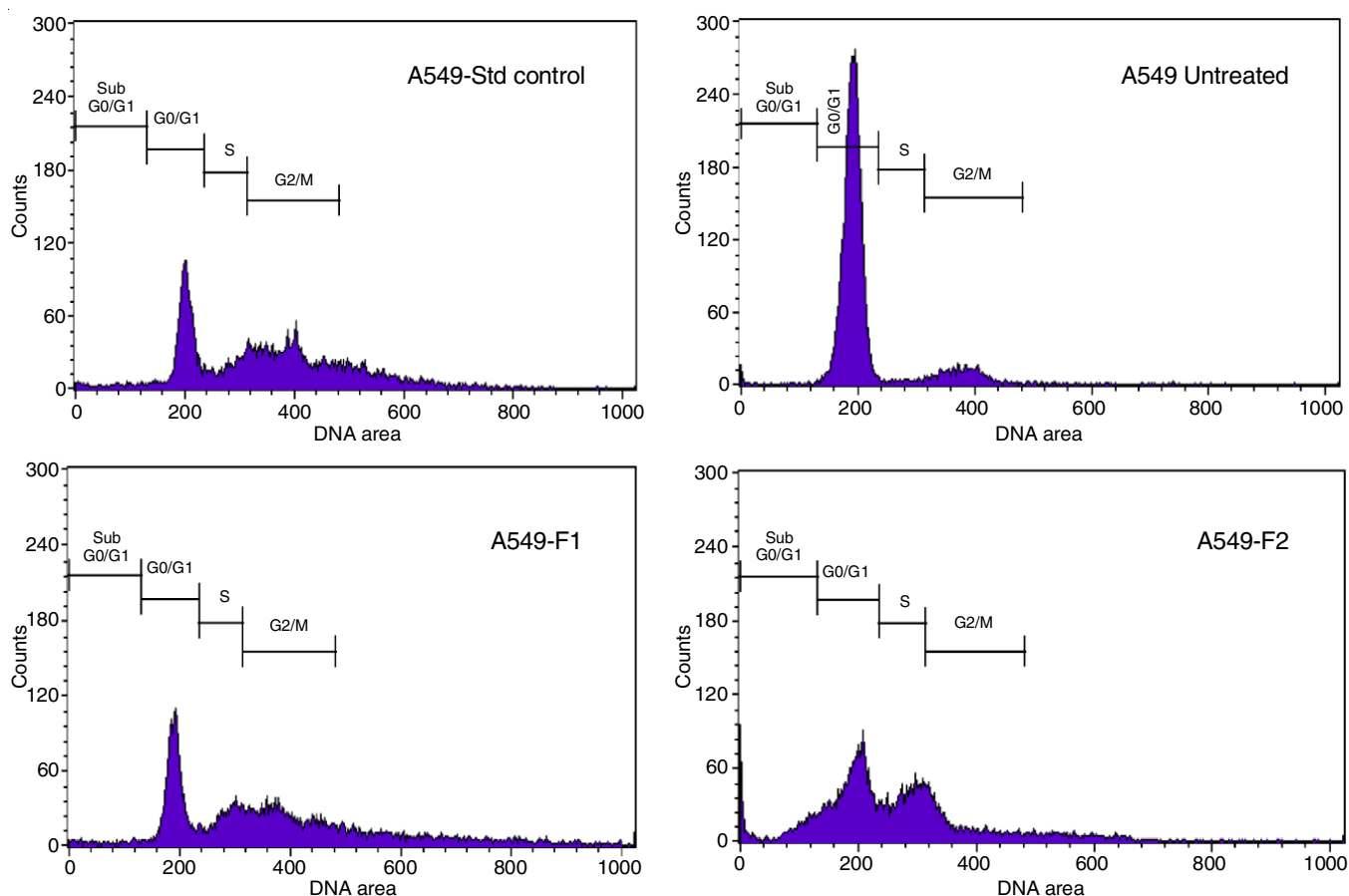


Fig. 9a. Flow cytometric histograms depicting the phases of cell cycle distribution in the A549 cell line treated with test compounds, FAP-M (F1) and FAP-P NPs (F2) with  $IC_{50}$  concentrations and standard drug, mangiferin at  $20 \mu\text{g}/\text{mL}$  concentration compared to the untreated control

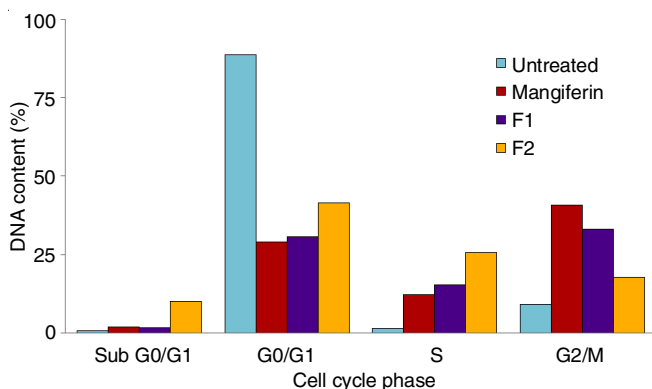


Fig. 9b. Graph showing the % of Cells get arrested in the different stages of a549 cell cycle after the treatment of test compounds, Mangiferin in comparison to the untreated cells. (F1: FAP-M NPs; F2: FAP-P NPs)

**Apoptosis assay:** The test chemicals, FAP-M NPs (F1), FAP-P NPs (F2) and mangiferin (control), significantly increased cell mortality after 48 h of nanoparticle treatment in A549 cells as compared to the untreated control and at  $IC_{50}$  levels. When compared to two A549 cells treated with FAP NPs, which exhibited high apoptotic activity against A549, the reference cells showed no indications of mortality. As an alternative, the FAP-M NPs and FAP-P NPs showed effective apoptotic capability after 48 h at the  $IC_{50}$  value (Table-7).

% Population of cells	Necrosis	Late apoptosis	Live	Early apoptosis
Untreated	0	0	99.8	0.2
Control	3.26	36.77	50.19	9.78
F1 with $IC_{50}$ conc.	12.9	32.58	45.75	8.77
F2 with $IC_{50}$ conc.	9.71	51.08	36.94	2.27

## Conclusion

Polymeric nanoparticles were synthesized through folic acid modification, facilitating their utilization for drug delivery. The encapsulation of mangiferin and piperine within these nanoparticles allowed for targeted delivery to drug-resistant sites within lung cancer cells. Furthermore, these nanoparticles exhibited favourable characteristics such as small size and high drug entrapment capacity. The gradual release of mangiferin and piperine from the nanoparticles resulted in a sustained therapeutic effect. *In vitro* experiments confirmed the cytotoxicity of mangiferin and piperine-loaded nanoparticles towards A549 lung cancer cells. This effect was corroborated by various assessments including the apoptosis assay, DNA fragmentation assay, tumorsphere assay and cell cycle assay. Consequently, our formulated nanoparticles hold promise as

an effective strategy for delivering mangiferin and piperine drugs. Extensive investigations conducted on different cell lines further established the safety and efficacy of the developed nanoparticulate formulation. Therefore, the combination of mangiferin and piperine drugs represents a highly viable approach for targeted drug delivery. Based on these compelling findings, these formulations present a potential option for *in vivo* drug delivery systems, utilizing polymeric nanoparticles loaded with mangiferin and piperine.

### CONFLICT OF INTEREST

The authors declare that there is no conflict of interests regarding the publication of this article.

### REFERENCES

- L.A. Nagahara, J.S. Lee, L.K. Molnar, N.J. Panaro, D. Farrell, K. Ptak, J. Alper and P. Grodzinski, *Cancer Res.*, **70**, 4265 (2010); <https://doi.org/10.1158/0008-5472.CAN-09-3716>
- R. Misra, S. Acharya and S.K. Sahoo, *Drug Discov. Today*, **15**, 842 (2010); <https://doi.org/10.1016/j.drudis.2010.08.006>
- S.C. Kamran and A.V. D'Amico, *Hematol. Oncol. Clin. North Am.*, **34**, 45 (2020); <https://doi.org/10.1016/j.hoc.2019.08.017>
- J. Liu, Y. Zheng and N. Xu, *Medicine*, **98**, 14328 (2019); <https://doi.org/10.1097/MD.00000000000014328>
- N. Muhamad, T. Plengsuriyakarn and K. Na-Bangchang, *Int. J. Nanomedicine*, **13**, 3921 (2018); <https://doi.org/10.2147/IJN.S165210>
- S. Parveen and S.K. Sahoo, *J. Drug Target.*, **16**, 108 (2008); <https://doi.org/10.1080/10611860701794353>
- X. Wang, L. Yang, Z.G. Chen and D.M. Shin, *CA Cancer J. Clin.*, **58**, 97 (2008); <https://doi.org/10.3322/CA.2007.0003>
- H. Maeda, J. Wu, T. Sawa, Y. Matsumura and K. Hori, *J. Control. Release*, **65**, 271 (2000); [https://doi.org/10.1016/S0168-3659\(99\)00248-5](https://doi.org/10.1016/S0168-3659(99)00248-5)
- G. Kaul and M. Amiji, *Pharm. Res.*, **19**, 1061 (2002); <https://doi.org/10.1023/A:1016486910719>
- C.E. Ashley, E.C. Carnes, G.K. Phillips, D. Padilla, P.N. Durfee, P.A. Brown, T.N. Hanna, J. Liu, B. Phillips, M.B. Carter, N.J. Carroll, X. Jiang, D.R. Dunphy, C.L. Willman, D.N. Petsev, D.G. Evans, A.N. Parikh, B. Chackerian, W. Wharton, D.S. Peabody and C.J. Brinker, *Nat. Mater.*, **10**, 389 (2011); <https://doi.org/10.1038/nmat2992>
- M.M. El-Hammadi, A.V. Delgado, C. Melguizo, J.C. Prados and J.L. Arias, *Int. J. Pharm.*, **516**, 61 (2017); <https://doi.org/10.1016/j.ijpharm.2016.11.012>
- M. de Sousa, L.A. Visani de Luna, L.C. Fonseca, S. Giorgio and O.L. Alves, *ACS Appl. Nano Mater.*, **1**, 922 (2018); <https://doi.org/10.1021/acsanm.7b00324>
- F. Gold-Smith, A. Fernandez and K. Bishop, *Nutrients*, **8**, 396 (2016); <https://doi.org/10.3390/nu8070396>
- S.N. Morozkina, T.H.N. Vu, Y.E. Generalova, P.P. Snetkov and M.V. Uspenskaya, *Biomolecules*, **11**, 79 (2021); <https://doi.org/10.3390/biom11010079>
- S.S. Katiyar, E. Muntimadugu, T.A. Rafeeqi, A.J. Domb and W. Khan, *Drug Deliv.*, **23**, 2608 (2016); <https://doi.org/10.3109/10717544.2015.1039667>
- A. Debbarma, K.R.P. Roy, T.C. Lalhriatpuii and H. Lalhlemawia, *Int. J. Pharm. Sci. Res.*, **14**, 1819 (2023); [https://doi.org/10.13040/IJPSR.0975-8232.14\(4\).1819-27](https://doi.org/10.13040/IJPSR.0975-8232.14(4).1819-27)
- C. Gibson, J. Gibson, I. Rosenberg and S. Ott, *Bioeng. Biotechnol.*, **8**, 1 (2020); <https://doi.org/10.12970/2311-1755.2020.08.01>
- A. Garg, G. Rai, S. Lodhi, A.P. Jain and A.K. Yadav, *Drug Deliv.*, **1**, 11 (2014).
- F.F. Razura-Carmona, A. Pérez-Larios, N. González-Silva, M. Herrera-Martínez, L. Medina-Torres, S.G. Sáyago-Ayerdi and J.A. Sánchez-Burgos, *Cancers*, **11**, 1965 (2019); <https://doi.org/10.3390/cancers11121965>
- I. Kazmi, F.A. Al-Abbasi, S.S. Imam, M. Afzal, M.S. Nadeem, H.N. Altayb and S. Alshehri, *Polymers*, **14**, 1349 (2022); <https://doi.org/10.3390/polym14071349>
- A. Mukerjee and J.K. Vishwanatha, *Anticancer Res.*, **29**, 3867 (2009).
- D. Venkataramana and D. Krishna, *J. Chromatogr. Biomed. Appl.*, **575**, 167 (1992); [https://doi.org/10.1016/0378-4347\(92\)80520-Z](https://doi.org/10.1016/0378-4347(92)80520-Z)
- V. Dua, P. Kar, R. Sarin and V. Sharma, *J. Chromatogr. Biomed. Appl.*, **675**, 93 (1996); [https://doi.org/10.1016/0378-4347\(95\)00357-6](https://doi.org/10.1016/0378-4347(95)00357-6)
- R.S. Douglas, A.D. Tarshis, C.H. Pletcher Jr., P.C. Nowell and J.S. Moore, *J. Immunol. Methods*, **188**, 219 (1995); [https://doi.org/10.1016/0022-1759\(95\)00216-2](https://doi.org/10.1016/0022-1759(95)00216-2)
- R.F. Kalejta, T. Shenk and A.J. Beavis, *Cytometry*, **29**, 286 (1997); [https://doi.org/10.1002/\(SICI\)1097-0320\(19971201\)29:4<286::AID-CYTO4>3.0.CO;2-8](https://doi.org/10.1002/(SICI)1097-0320(19971201)29:4<286::AID-CYTO4>3.0.CO;2-8)
- I. Vermes, C. Haanen, H. Steffens-Nakken and C. Reutellingsperger, *J. Immunol. Methods*, **184**, 39 (1995); [https://doi.org/10.1016/0022-1759\(95\)00072-1](https://doi.org/10.1016/0022-1759(95)00072-1)
- M. Danaei, M. Dehghankhold, S. Ataei, F.H. Davarani, R. Javanmard, A. Dokhani, S. Khorasani and M.R. Mozafari, *Pharmaceutics*, **10**, 57, (2018); <https://doi.org/10.3390/pharmaceutics10020057>
- A. Garg, G. Rai, S. Lodhi, A.P. Jain and A.K. Yadav, *Int. J. Biol. Macromol.*, **87**, 449 (2016); <https://doi.org/10.1016/j.ijbiomac.2015.11.094>